

1 **Running Head: Phased Target Enrichment for Polyploids**

2 **Phasing Alleles Improves Network Inference with Allopolyploids**

3 George P. Tiley^{1,†,*}, Andrew A. Crowl^{1,†}, Paul S. Manos¹, Emily B. Sessa², Claudia Solís-
4 Lemus³, Anne D. Yoder¹, J. Gordon Burleigh²

5 ¹Department of Biology, Duke University, Durham NC, 27708, USA

6 ²Department of Biology, University of Florida, Gainesville FL, 32611, USA

7 ³Wisconsin Institute for Discovery and Department of Plant Pathology, University of Wisconsin –
8 Madison, Madison WI, 53706, USA

9 [†]These authors contributed equally

10 ^{*}Author for correspondence: george.tiley@duke.edu

11

12

13 **Abstract**

14 Accurately reconstructing the reticulate histories of polyploids remains a central
15 challenge for understanding plant evolution. Although phylogenetic networks can provide
16 insights into relationships among polyploid lineages, inferring networks may be hampered by the
17 complexities of homology determination in polyploid taxa. We use simulations to show that
18 phasing alleles from allopolyploid individuals can improve inference of phylogenetic networks
19 under the multispecies coalescent. Phased allelic data can also improve divergence time
20 estimates for networks, which is helpful for evaluating allopolyploid speciation hypotheses and
21 proposing mechanisms of speciation. To achieve these outcomes, we present a novel pipeline
22 that leverages a recently developed phasing algorithm to reliably phase alleles from polyploids.
23 This pipeline is especially appropriate for target enrichment data, where depth of coverage is
24 typically high enough to phase entire loci. We provide an empirical example in the North
25 American *Dryopteris* fern complex that demonstrates how phasing can help reveal the mode of
26 polyploidization and improve network inference. We establish that our pipeline (PATÉ: Phased
27 Alleles from Target Enrichment data) is capable of recovering a high proportion of phased loci
28 from both diploids and polyploids, and that these data improve network estimates compared to
29 using haplotype consensus assemblies. This approach is shown to be especially effective in
30 reticulate complexes where there are multiple hybridization events. The pipeline is available at:
31 <https://github.com/gtiley/Phasing>.

32

33 **Key words:** Introgression; Hybridization; Reticulate Evolution; Multispecies Coalescent;
34 Divergence Time Estimation; Polyploidy; Target Enrichment; *Dryopteris*

35

36

37 INTRODUCTION

38 The phenomenon of polyploidy, or whole-genome duplication, occurs throughout the tree
39 of life. Nowhere, perhaps, is its evolutionary significance more evident than in plants, with recent
40 estimates suggesting up to 35% of vascular plant species are of recent polyploid origin (Wood
41 et al. 2009; Barker et al. 2016). Despite advances in genomic data generation and a long-term
42 interest in understanding the role of whole-genome duplication in driving plant speciation and
43 local adaptation (reviewed in Soltis et al. 2014), polyploids remain a central challenge for the
44 field of phylogenetics. One persistent problem when analyzing sequence data from polyploid
45 taxa, and especially allopolyploids, is identifying the alleles and divergent homeolog copies from
46 parental lineages. Most bioinformatic tools for processing next generation sequence data were
47 developed with diploids, or specifically humans, in mind. These approaches often collapse
48 variable homeolog sequences into a single consensus sequence for *de novo* assemblies or
49 assume the organism is diploid when performing genotyping and phasing for reference-based
50 assembly. For polyploids, this creates chimeric sequences that may interfere with phylogenetic
51 reconstruction and obscure signals of polyploidy and polyploid mode-of-origin. Using allelic data
52 that more accurately capture the complex genomic histories of polyploids should enable the
53 incorporation of divergent signals from polyploid loci into phylogenomic inference, distinguish
54 allopolyploidy from autopolyploidy, and identify parental taxa. However, few studies have
55 examined the potential benefits of using phased versus unphased data to reconstruct polyploid
56 histories, and there are few formal methods and little guidance for phasing alleles from polyploid
57 taxa. Here we explore the value of using phased data to reconstruct polyploid networks
58 leverage recent algorithmic advances in polyploid phasing (Xie et al. 2016) to develop a
59 bioinformatic pipeline that can phase alleles from polyploids using target enrichment sequence
60 data.

61 Previous studies of reticulate complexes have suggested phasing alleles is crucial for
62 accurate evolutionary reconstruction, at least when sampling relatively few loci (e.g., 4 to 10;

63 Rothfels et al. 2017; Eriksson et al. 2018). The applications of phased sequencing data for
64 phylogenomic studies of polyploid complexes are thus enticing; however, it remains challenging
65 to genotype and phase next generation sequencing data from polyploids. Methods exist to
66 genotype consensus loci from target enrichment data, but these have been either limited to
67 diploids (Kates et al. 2018; Andermann et al. 2019) or manual curation of variants with
68 polyploids where both parental populations are available (Eriksson et al. 2018). Otherwise,
69 obtaining phased sequence data for polyploids has largely depended on costly long-read
70 sequencing to recover complete haplotype sequences (e.g., Rothfels et al. 2017), or cloning
71 PCR products (e.g., Sessa et al. 2012; Oberprieler et al. 2017).

72 Target enrichment (or HybSeq), where specific regions of the genome are isolated and
73 sequenced (Faircloth et al. 2012; Lemmon et al. 2012), is an increasingly common method for
74 collecting large-scale phylogenomic datasets, and these data can provide insights into the
75 evolutionary history of reticulate complexes (e.g., Crowl et al. 2017; Karimi et al. 2020) and
76 sources of gene tree discordance (e.g., Morales-Briones et al. 2018; Stull et al. 2020). Probe
77 kits for target enrichment have been developed in many land plant lineages (Wolf et al. 2018;
78 Johnson et al. 2019; Liu et al. 2019; Breinholt et al. 2021), and there are bioinformatic pipelines
79 available for custom probe design (e.g., Jantzen et al. 2020). The most common approach to
80 assemble phylogenetic datasets from target enrichment data has been to use *de novo* assembly
81 pipelines (Faircloth 2016; Johnson et al. 2016; Andermann et al. 2018; Breinholt et al. 2018).
82 The assembly algorithms within these pipelines typically treat variable base calls as sequencing
83 errors and consider only the most frequent nucleotide sequence while discarding the
84 alternatives (Bankevich et al. 2012; Iqbal et al. 2012; Luo et al. 2012). This results in loci in
85 which variable positions are collapsed to a single base call (haplotype consensus loci), losing
86 information related to heterozygosity. While this may be appropriate, or at least benign, for
87 phylogenetic analyses of diploid taxa (Kates et al. 2018), it may pose substantial problems when
88 attempting to investigate the evolutionary history of polyploid taxa or reticulate lineages.

89 While phylogenetic studies in plants often infer strictly bifurcating trees, the complexities
90 of allopolyploid evolution can be represented more accurately using networks. Simulations and
91 empirical analyses have suggested that phylogenetic networks can recover the reticulate
92 histories of polyploid lineages with few loci, at least when gene tree discordance due to
93 incomplete lineage sorting (ILS; Hudson et al. 1983; Pamilo and Nei 1988) is low (Oberprieler et
94 al. 2017) using parsimony methods (Huber et al. 2006; Lott et al. 2009), or even with moderate
95 ILS when explicitly modeled (Jones et al. 2013). Contemporary phylogenetic network models
96 and software packages jointly consider gene tree variation due to allele sampling error as
97 described by the multispecies coalescent (MSC; Rannala and Yang 2003) and gene flow
98 modeled as episodic introgression events (Solis-Lemus and Ané 2016; Wen et al. 2016; Zhang,
99 Ogilvie et al. 2018, Flouri et al. 2020). Depending on the complexity and goals of the research
100 question, these methods can search for networks with a constrained number of reticulation
101 events using quartet-based maximum pseudolikelihood (Solis-Lemus and Ané 2016; Wen et al.
102 2018) or a full-likelihood Bayesian model where the number of reticulations is a parameter (Wen
103 et al. 2018; Zhang et al. 2018). Also, it is possible to estimate model parameters (divergence
104 times, population sizes, and the fraction of introgressed genes) on a fixed species network using
105 a full-likelihood Bayesian model that allows efficient computation with large numbers of loci
106 (Flouri et al. 2020). We refer to these network models from here on as the multispecies
107 coalescent with introgression (MSci), consistent with Flouri et al. (2020); although, other names
108 have been used, such as the network multispecies coalescent (NMSC; e.g. Zhu and Degnan
109 2017) and multispecies network coalescent (MSNC; e.g., Wen et al. 2016). We emphasize that
110 network approaches to investigate polyploid complexes are not novel (e.g., Huber et al. 2006;
111 Lott et al. 2009; Jones et al. 2013), but the difficulty of collecting appropriate genomic data from
112 polyploids for such analyses has limited their use.

113 To address the issues outlined above, we have developed a pipeline, PATÉ (Phased
114 Alleles from Target Enrichment data), that can phase genotyping data for individuals of a known

115 ploidy without the need for sampling their parental lineages. PATÉ was designed with scalability
116 and population-level sampling in mind for target enrichment projects where deep coverage from
117 paired-end Illumina data allow calling of high-quality variants. In this study, we first use
118 simulations to explore the ability of network approaches to reconstruct the history of
119 allopolyploidy in the presence of ILS, and whether phasing the data affects the accuracy of the
120 reconstruction. We show that using phased allelic data can improve network estimation and
121 divergence time estimation compared to using haplotype consensus sequences, but also
122 highlight scenarios where phasing may not be necessary or beneficial. Next, we describe the
123 individual steps used by PATÉ to phase target enrichment data. For an empirical example of the
124 benefits of PATÉ, we compare phased and unphased (haplotype consensus) data to infer the
125 evolutionary history of the North American *Dryopteris* complex, a model system for reticulate
126 polyploid evolution (Sessa et al. 2012a; Sessa et al. 2012b), using new targeted enrichment
127 data. The system includes four diploid species, as well as one extinct diploid, that have formed
128 five allopolyploids in which there is high confidence in the parent-progeny relationships (Fig. 1),
129 although numerous sterile allopolyploid species have also been reported within the complex
130 (Montgomery and Paulton 1981). The allopolyploid species have relatively ancient origins, with
131 the best estimates placing hybridization events between six and 13 Ma (Sessa et al. 2012b).
132 PATÉ is largely successful in recovering phased haploid sequences from polyploid individuals,
133 and networks inferred from phased data more accurately represent the North American
134 *Dryopteris* complex than those inferred from unphased data.

135

136 **MATERIALS & METHODS**

137 ***Testing the Effects of Phasing on Network Inference through Simulation***

138 *Simulating phased and unphased sequence data for an allopolyploid* — We simulated
139 gene trees and their nucleotide sequence data using the MSC model with BPP v1.4.1 (Flouri et
140 al. 2018) under a five-species network (Fig. 2). All simulations used the Jukes-Cantor (Jukes

141 and Cantor 1969) model of sequence evolution with no rate heterogeneity. The allopolyploid
142 species E was treated as two lineages (E sister to B and F sister to C) whose alleles were
143 pooled to form the hybrid species E at time τ_h . This makes species E a tetraploid hybrid with the
144 parents B and C . θ was constant among lineages and set at 0.01. Assuming a per-generation
145 mutation rate (μ) of 1×10^{-8} and one year per generation yields an effective population size
146 (N_e) of 250,000 and root age of 10 Ma for the simulation network (Fig. 2). We also simulated
147 data under a shallow divergence scenario, in which all node ages were divided by 10, and a
148 deep divergence scenario, in which all node ages were multiplied by 10. This changes the root
149 age (τ_r) to 0.01 (1 Ma) and 1.0 (100 Ma), respectively.

150 Because the distance between speciation nodes is 0.025 and $\theta = 0.01$ for the simulation
151 network (Fig. 2), there are five coalescent units between nodes, $T = \frac{\tau}{\left(\frac{\theta}{2}\right)}$ (Yang 2006), which
152 implies a near-zero probability of gene tree discordance due to ILS (Hudson 1983). We
153 incorporated ILS into the simulation by reducing the node heights τ_u and τ_s to 0.0375 and 0.05
154 (for a low level of ILS) and 0.03 and 0.035 (for a moderate level of ILS). This increases the
155 probability of ILS at node u and s to 0.05 and 0.25, respectively. Thus, we used a total of nine
156 simulation conditions that combined three levels of evolutionary distance and three levels of ILS.
157 While our simulations do not explore extreme levels of gene tree discordance, they allow us to
158 learn about some general features of increasing ILS on network inference with different data
159 types. We simulated 1000 gene trees and their sequences, 500bp in length, under the MSC for
160 each of the nine conditions. We also explored the effects of sampling fewer genes on
161 downstream analyses. For each replicate of 1000 gene trees and their sequences, we randomly
162 sampled 400, 40, and four genes without replacement.

163 All simulations sampled haploid data. Two haploid sequences were sampled for each
164 diploid species and four haploid sequences were sampled for the allopolyploid species E , where
165 two sequences came from each parental lineage. We then investigated unphased data in three

166 ways. First, to generate unphased genotype sequences, the simulated haploid sequences for
167 each species were collapsed into a single sequence in which heterozygous sites were
168 represented by IUPAC ambiguity codes (genotype). The allopolyploid species was not restricted
169 to only biallelic sites. Second, we generated haploid consensus sequences, where for each
170 variable site, only one base was randomly retained (consensus). This could represent a case in
171 which read coverage across a locus is highly uneven such that a haploid sequence is actually a
172 chimera of two or more alleles. Finally, we simply picked one phased haploid sequence, which
173 is possible when one parental haplotype has a majority of reads for a locus (pick one). This
174 scenario where only one parent's sequence would be recovered in the offspring could be
175 anticipated in real data due to subgenome dominance (e.g., Buggs et al. 2014; Bird et al. 2018).
176 In practice, we expect most *de novo* assemblers to generate output in between the haploid
177 consensus data and pick one data.

178

179 *Inferring species networks with phased and unphased simulated data* — We estimated
180 species networks with PhyloNetworks v0.12.0 (Solis-Lemus et al. 2017) using Julia v.1.4.1
181 (Bezanson et al. 2015) from either the true gene trees used to simulate the data, or gene trees
182 estimated from the phased or unphased sequence data. For estimated trees, we used IQTREE
183 v1.6.10 (Nguyen et al. 2015) with the same model used for simulation. Each PhyloNetworks
184 analysis used the species tree (A,((B,E),(C,D))) as the starting tree and allowed zero, one, or
185 two reticulation events. Each analysis included ten independent optimizations of the
186 pseudolikelihood score. We considered larger numbers of reticulations an improvement if they
187 were two or more pseudolikelihood units lower than the best model. We compared the
188 estimated networks with one reticulation to the true network with the *hardwiredClusterDistance*
189 function (Huson et al. 2010) in PhyloNetworks. This allowed us to score the number of
190 replicates that 1) recovered the correct number of reticulations and 2) matched the true network
191 when the number of reticulations was set to one. We estimated networks for samples of four,

192 40, 400, and 1000 gene trees for each of the 30 replicates for each of the nine simulation
193 divergence and ILS conditions.

194

195 *Effect of phasing on divergence time estimation* — We also used our simulated phased
196 and unphased data to estimate divergence times under the MSci model (Flouri et al. 2020)
197 using BPP v4.2.9. Here, we estimate divergence times (τ_s), population sizes (θ_s), and the
198 proportion of introgressed loci (φ) on the correct fixed species network. MSci analyses used
199 diffuse priors on τ_r and θ with a mean on their simulated values with $\varphi \sim \beta(1,1)$. Phased,
200 consensus, and pick one sequences were treated as haploids while genotype sequences were
201 treated as unphased diploids and used the analytical phasing (Gronau et al. 2011) implemented
202 in BPP. Although this is not correct for the tetraploid, it is arguably more appropriate than
203 treating all of the genotype sequences as haploid. Each Markov chain Monte Carlo (MCMC)
204 analysis collected 10,000 posterior samples, saving every 100 generations, while discarding the
205 first 100,000 generations (i.e., 10% of the total run) as burnin. All scripts for simulation and
206 subsequent analyses of simulated data are available in Dryad (X).

207

208 ***A Phasing Pipeline for Polyploids***

209 *Target enrichment data* — We were motivated by the general premise of using phased
210 data to infer reticulate evolutionary histories of polyploids based on the success of empirical
211 studies where phasing was informative about hybridization or introgression events (e.g.,
212 Oberprieler et al. 2017; Eriksson et al. 2018). We were aware of few instances of phasing
213 genomic or phylogenomic data in polyploids, except in cases where chromosome-level whole-
214 genome assemblies have characterized subgenomes in allopolyploid crops (Yang et al. 2017;
215 Colle et al. 2019) or emerging results that are dependent on the sampling of parental lineages
216 (Freyman et al. 2020; Nauheimer et al. 2020). We designed PATÉ for target enrichment data

217 because of the availability of such data for many of taxa, but it is applicable to other types of
218 data with paired-end Illumina reads.

219 The end product of a *de novo* target enrichment assembly pipeline (such as HybPiper;
220 Johnson et al. 2016) generally is a single consensus sequence for each locus for each
221 individual. Allelic variation may be represented by ambiguous nucleotide codes within the single
222 consensus sequence or lost when the pipeline outputs the haplotype consensus sequence
223 where the majority vote from a collection of reads is used. We use these existing *de novo*
224 assembly pipelines as a starting point to provide the reference sequence for each locus for each
225 individual and leverage a recent phasing algorithm with high-quality variant calls to recover
226 phased haplotype sequences for taxa with known ploidy levels. Ploidy levels were well-
227 characterized for individuals in our *Dryopteris* analyses, but for unknown systems there are
228 existing methods to estimate ploidy directly from target enrichment data (Weiss et al. 2018;
229 Viruel et al. 2019) in the absence of other sources, such as flow cytometry (Farhat et al. 2019).

230

231 *Phasing alleles within loci* — PATÉ (Fig. 3) starts with assembled target enrichment loci,
232 such as the supercontig files output from HybPiper (Johnson et al. 2016) that contain a single
233 haplotype consensus sequence from each individual per locus. Reads for each individual are
234 then realigned to their consensus locus using BWA v0.7.17 (Li and Durbin 2009). PCR
235 duplicates are flagged with MarkDuplicates in Picard v2.9.2
236 (<http://broadinstitute.github.io/picard>), and variant calls are computed with HaplotypeCaller in
237 GATK v.4.1.4 (McKenna et al. 2010). We applied the following hard filters with VariantFiltration
238 in GATK: (1) QD < 2.0, (2) FS > 60.0, (3) MQ < 40.0, (4) ReadPosRankSum < -8.0, (5) AF <
239 0.05 || AF > 0.95. These loosely follow community recommendations on filters for germline
240 variant discovery (DePristo et al. 2011). Notably, we do not perform quality score recalibration
241 or filter on the mapping quality rank sum, as we anticipate allopolyploids could have a lower
242 mapping quality associated with an alternate allele due to sequence divergence or structural

243 variation among homeologous chromosomes. We also consider a very narrow window for
244 filtering on allele frequency. Because increasing ploidy levels will generate smaller anticipated
245 ratios of alternate to reference alleles, coupled with sequencing error and read stochasticity, we
246 only aim to remove the most extreme cases. For example, if almost all reads support the
247 alternate allele at a site, it is difficult to diagnose if the error lies in the consensus assembly or
248 the read alignment. In these cases, only the reference site is retained, and the variant does not
249 pass the allele frequency filter. However, the allele frequency filter could be removed if
250 investigators are focused on organisms with extremely high ploidy levels.

251 Biallelic SNPs that pass filters are then phased with H-PoPG v.0.2.0 (Xie et al. 2016). H-
252 PopG solves a heuristic phasing problem efficiently using dynamic programming. Although not
253 guaranteed to be an optimal solution, H-PoPG has been shown to have high accuracy while
254 also being fast (Xie et al. 2016; He et al. 2018; Moeinzadeh et al. 2020). Phasing variants in
255 polyploids is difficult because for n variants and k ploidy, there are $2^{n-1}(k-1)^n$ possible ways
256 to link the sites together. H-PoPG evaluates possible solutions efficiently by grouping reads into
257 k groups in such a way that differences within the groups are minimized. Focusing on target
258 enrichment data also constrains the complexity of the phasing problem compared to whole-
259 genome alignments (i.e., haplotype blocks are constrained to about 1000 bp). We then used the
260 phased variants to create individual allele sequences, where invariable sites are filled in based
261 on the reference sequence. In cases where there is no linkage information to phase across the
262 entire locus, we retain the phasing only for the longest block. The variants for the shorter
263 haplotype blocks can be collapsed into IUPAC ambiguity codes or treated as missing data
264 based on the investigator's preferences. PATÉ outputs analysis-ready fasta files with multiple
265 alleles per species. Variants are only phased within loci; we do not attempt to assign loci to
266 parental subgenomes. While this may complicate analyses of concatenated multi-locus
267 datasets, it is ideal for the MSC that assumes free recombination between loci and can leverage
268 multiple alleles per species for estimating θ_s . Those interested in concatenated analyses can

269 use other recent approaches that assign gene copies to parental subgenomes (Freyman et al.
270 2020; Nauheimer et al. 2020).

271

272 ***Analyses of a Species Complex with Allopolyploidy***

273 *The North American wood fern complex (Dryopteris)* — We tested PATÉ using new
274 target enrichment data from nine North American *Dryopteris* species, including both
275 allotetraploid and allohexaploid taxa, with well-studied reticulate relationships (Sessa et al.
276 2012a, b) as well as two outgroup taxa from the sister genus *Polystichum*. All putative parental
277 lineages are represented in our dataset, with the exception of a hypothesized extinct lineage (*D.*
278 *semicristata*; Sessa et al. 2012b). We sampled two or three individuals for each *Dryopteris*
279 taxon (Table S1). The target enrichment data were generated from the GoFlag 408 flagellate
280 land plant probe set (Breinholt et al. 2021) at RAPID Genomics (Gainesville, FL). The target
281 regions for this probe set are 408 exons found in 229 single or low-copy nuclear genes. We
282 generated haplotype consensus assemblies for each with HybPiper (Johnson et al. 2016). The
283 resulting supercontig sequences became our reference sequences for genotyping and phasing
284 with PATÉ. We aligned both phased and unphased (i.e., the reference supercontig sequences)
285 with MUSCLE with default settings (Edgar 2004).

286

287 *Three species tests* — We first explored the value of phasing data when estimating
288 reticulate relationships among three species, including two diploid parental lineages (*D.*
289 *expansa* and *D. intermedia*) and their putative allotetraploid descendent (*D. campyloptera*). The
290 two diploid parents last shared a common ancestor during the Late Eocene and Early Miocene,
291 approximately 23 Ma (Sessa et al. 2012b). We used both a full-likelihood Bayesian approach
292 and a topology-based pseudolikelihood approach to estimate the correct species relationships
293 from phased and unphased data. First, using BPP v.4.1.4 (Flouri et al. 2020), we estimated log-
294 marginal likelihoods ($\ln mL$) with stepping-stone sampling (Xie et al. 2011) for the three possible

295 rooted three taxon trees and twelve possible network models that imply differences for the
296 timing and direction of allopolyploidy and the presence of unsampled ancestral lineages
297 (Supplementary Fig. S1). Each $\ln mL$ estimate used 24 steps, and each step had a posterior
298 sample of 10,000, saving every 100 generations after a 100,000 generation burnin (10% of the
299 total run). The $\ln mL$ values were then used to calculate the fifteen model probabilities following
300 equation 1 (e.g., Beerli et al. 2019).

$$301 \quad P(model) = \frac{\exp(\ln mL_{model} - \ln mL_{max})}{\sum_i [\exp(\ln mL_i - \ln mL_{max})]} \quad Equation 1$$

302 We repeated analyses for 30 random subsets of 40 and then four loci to explore the
303 effects of the number of loci on inferring allopolyploidy. Next, we used PhyloNetworks to test the
304 presence and placement of gene flow between the three species. For that analysis, we also
305 included the sequences from the two *Polystichum* outgroups. IQ-TREE v1.6.10 (Nguyen et al.
306 2015) and model selection by ModelFinder (Kalyaanamoorthy et al. 2017) was used to estimate
307 gene trees for the phased and unphased data. The starting tree was obtained with ASTRAL III
308 v5.6.3 (Zhang, Rabiee et al. 2018). We tested the presence of zero, one, or two reticulations
309 with slope heuristics (Solis-Lemus and Ané 2016). Each analysis used ten independent
310 optimizations. In addition to the dataset of all loci, we analyzed the same 30 random subsets of
311 40 and four loci from the marginal likelihood analyses.

312
313 *Nine species tests* — We also investigated the differences in results from phased versus
314 consensus sequences when estimating a network for the nine-species complex, which involves
315 multiple reticulation events on an edge and thus should be difficult for network estimation (Solis-
316 Lemus and Ané 2016). Because the increased number of species and complexity of reticulation
317 in *Dryopteris*, evaluation with marginal likelihoods was not computationally feasible. Instead, we
318 performed analyses of the nine-species complex and two outgroups with phased and unphased
319 haplotype consensus data with PhyloNetworks as described above, but we allowed up to six

320 reticulation events. We used ASTRAL III v5.6.3 (Zhang, Rabiee et al. 2018) to generate the
321 starting species tree for network estimation using gene trees inferred from IQ-TREE v1.6.10
322 (Nguyen et al. 2015) with the best model selected by ModelFinder (Kalyaanamoorthy et al.
323 2017).

324

325 **RESULTS**

326 ***Simulation Shows Benefits of Phased Data***

327 *Network inference* — In our simulation results, both phased (i.e., the haplotypic allele
328 sequences) and unphased data (i.e., genotype, consensus, and pick one) performed well when
329 the goal is only to detect the correct number of reticulations (Supplementary Fig. S2). The only
330 case where analyses did not converge to the true number of reticulations was in the presence of
331 moderate ILS and high nucleotide divergence; however, this appears largely due to gene tree
332 estimation error, as analyses using the true simulated gene trees greatly outperformed those
333 using gene trees estimated from the simulated sequence data. However, using phased data
334 provides more accurate estimates of the placement of the reticulation edge in comparison to
335 using genotype data, and to a lesser extent, consensus sequences (Fig. 4). When the true gene
336 trees were used, which have information about the allopolyploid's hybridization event (i.e., the
337 allele sequences are sister to their respective parents in every tree), the correct network can be
338 inferred with 40 or fewer loci when nucleotide divergence is moderate. The gene trees
339 estimated from phased data perform equally well, although they require a few more gene trees
340 when nucleotide divergence is low and ILS moderate. Analyses using the genotype data almost
341 never recover the true network for these medium and low divergence scenarios, regardless of
342 the amount of ILS. Analyses based on pick one data perform similarly well to the phased and
343 true data when sampling 400 loci, but they are less accurate for four or 40 loci at low and
344 medium divergences. Analyses using the consensus data perform poorly for low numbers of loci
345 under a low divergence and no ILS scenario, but they are capable of recovering the true

346 reticulation when sampling 400 or more loci for the other low and medium divergence cases. In
347 the high divergence simulations, all data types could infer the true network if enough genes
348 were sampled, but analyses with the phased data required fewer genes than others.

349

350 *Divergence times* — Using phased data also improves divergence time estimates when
351 nucleotide divergence is low, but not when divergence is moderate or high (Fig. 5). When
352 divergence was low, the timing of reticulate events was accurately estimated when using
353 phased haplotypic data, but was overestimated when using genotype and especially consensus
354 data. For analyses with genotype and consensus data, as the number of loci increased and
355 uncertainty in the posterior was reduced, the posterior mean did not converge to the true
356 estimate and the simulated value was not within the highest posterior density (HPD) interval.
357 Additionally, all other nodes in the species network were overestimated with genotype or
358 consensus data, while the phased data were capable of recovering the simulated divergence
359 times (Supplementary Figs. S3-S5). Aside from some cases with the consensus sequences, all
360 four data types performed similarly with four loci; however, this is likely due to the posterior
361 being dominated by the prior in the absence of enough data. There was little improvement in
362 divergence time estimates when going from 40 to 400 loci, aside from further reduction in the
363 HPD intervals.

364 For medium sequence divergence, there was little difference between the phased and
365 unphased data. Phased sequences slightly underestimated the timing of hybridization while
366 unphased data slightly overestimated the timing of these events. However, phased data
367 accurately estimated the age of older speciation nodes that were again systematically
368 overestimated with unphased data (Supplementary Figs. S6-S8). At a high level of nucleotide
369 divergence, genotype data were capable of accurately estimating all divergence time
370 parameters while the phased data underestimated the timing of hybrid events (Fig. 5;
371 Supplementary Figs. S9-S11). Notably, the pick one data performed very well for all divergence

372 time estimation scenarios. Divergence times were not strongly affected by increasing levels of
373 ILS, likely because estimates were performed with the MSci model and we did not explore very
374 high ILS scenarios, but age estimates improved slightly for the genotypes, consensus, and pick
375 one data with increasing ILS.

376

377 ***Analyses of target enrichment data from Dryopteris***

378 *Recovery of Phased Loci* — On average, 62% of loci sequenced for an individual were
379 phased with eight variants passing filters (Table S2). The ploidy level appears to be strongly
380 associated with the number of phased loci. Among diploids, only 30% of loci were phased; the
381 other 70% of diploid loci were either homozygous or had too few linked variants for phasing. For
382 tetraploids and hexaploids, 87% and 94% of loci, respectively, were phased such that two or
383 more phased haplotype sequences could be recovered. Among loci where phasing was
384 possible, variants were almost always resolved as a single haplotype block, as opposed to
385 being split into two or more blocks because not enough reads were available to physically link
386 variants. For polyploids, the number of phased haplotype sequences most frequently matched
387 the ploidy level except in the case of a single *D. campyloptera* individual (B087-D08), which also
388 had few recovered loci. Phasing data only extended sequence alignment length by about four
389 base pairs, but it more than doubled the number of parsimony informative sites (Table S3).

390

391 *Placing a single reticulation event* — For our three-species full-likelihood analyses with
392 the MSCi, both phased and unphased data recovered the anticipated reticulation hypothesis,
393 identifying *D. campyloptera* as an allotetraploid with the two diploid parental lineages *D.*
394 *expansa* and *D. intermedia*, when using all loci (Table 1). Model probabilities show decisive
395 support for a scenario where there are two unsampled ancestral populations that were the
396 progenitors of *D. campyloptera*, as opposed to *D. campyloptera* being a hybrid species with
397 extant *D. expansa* and *D. intermedia* as parents. All model parameters converged for both

398 phased (Supplementary Figs. S12 and S13) and unphased data (Supplementary Figs. S14 and
399 S15). Divergence time estimates were older in the analysis of phased data, although the relative
400 order of divergence events was the same using phased and unphased data (Fig. 6). There was
401 more uncertainty in the θ estimates, especially for the allopolyploid species *D. campyloptera* and
402 the two ancestral populations of the parental lineages that formed the polyploid ancestor
403 (Supplementary Figure S16). Repeating the analyses with fewer loci did not always produce the
404 same result, but there was either decisive support for a model or multiple plausible models that
405 all had the correct species relationships and direction of introgression for both phased and
406 unphased data when using 40 loci (Fig. 7). The only difference between models was the
407 presence or absence of ancestral θ_s for unsampled lineages. Analyses with four loci produced
408 less reliable results for both phased and unphased data. The four-locus analyses of phased and
409 unphased data found some non-negligible model probability for trees without hybridization or
410 networks where hybridization was incorrect in nine and twelve out of 30 replicates, respectively
411 (Fig. 7).

412 When performing a network search based on gene tree distributions, both the phased
413 and unphased data were able to recover the hypothesized allopolyploidy event (Fig. 8;
414 Supplementary Table S5). Both analyses inferred the major branch to be *D. intermedia* with the
415 minor branch from *D. expansa*. Phased data estimated a slightly smaller inheritance probability
416 compared to the unphased data. These findings from PhyloNetworks are consistent with
417 parameter estimation under the MSci model, where phased data estimated a slightly smaller
418 mean φ_h compared to unphased data (Table S4). When sampling 100 replicates of 40 loci, 98%
419 of replicates for phased data and 100% for unphased data were capable of detecting a single
420 hybrid event in the data. When sampling four loci, this drops to 66% and 85%, respectively (Fig.
421 8). Phased data more frequently recovered the correct network (58%) compared to unphased
422 data (38%) with 40 loci; however, the converse is true for four loci, with 34% correct for phased
423 and 41% correct for unphased (Fig. 8). Unphased data also got the network wrong more

424 frequently than phased data, such that phased data had the direction of introgression incorrect
425 in 36% and 12% of replicates while unphased data were incorrect in 60% and 38% replicates for
426 40 and four loci, respectively (Fig. 8).

427

428 *Inferring relationships among a complex with multiple reticulation events* — The network
429 recovered for phased data identified three out of five hypothesized reticulation events among
430 the nine *Dryopteris* species (Fig. 9; Supplementary Table S5). The allotetraploid *D. celsa* was
431 correctly identified with diploid *D. ludoviciana* and *D. goldiana* as parents. Analysis of the
432 phased data detected a low level of gene flow from the common ancestor of this clade into
433 tetraploid *D. cristata*, which has *D. ludoviciana* as one hypothesized parent while the other
434 parent lineage (*D. semicristata*) is assumed to be extinct (Sessa et al. 2012b). *Dryopteris*
435 *carthusiana* is another tetraploid that is assumed to share the extinct common ancestor with *D.*
436 *cristata*, but has experienced introgression from *D. intermedia*, with a high inheritance
437 probability of 0.43 (Fig. 9). However, the phased data missed the putative allotetraploid case of
438 *D. campyloptera*, despite the strong evidence for this reticulation event in our earlier three-taxon
439 analyses. Our network with phased data also failed to identify the putative reticulate
440 evolutionary history of *D. clintoniana*, an allohexaploid where allotetraploid *D. cristata* and
441 diploid *D. goldiana* are assumed to be the parents (Sessa et al. 2012b). The spectra of quartet
442 concordance factors were overall similar between the phased and unphased data
443 (Supplementary Fig. S17), but the phased data were arguably more accurate.

444 Although the phased data were not successful in recovering all hypothesized reticulate
445 relationships, they performed better than the unphased data. Analyses of unphased data were
446 capable of finding the allotetraploid history of *D. celsa* with an inheritance probability similar to
447 the phased data (Fig. 9). Hybridization between *D. intermedia* and *D. carthusiana* was also
448 detected; however, the directionality was reversed, with gene flow going from the allotetraploid
449 into the diploid. A third reticulation edge was found in the unphased analysis, from the common

450 ancestor of *Dryopteris* into the common ancestor of *D. clintoniana* and its sister clade. This
451 hybrid edge is difficult to reconcile because of the hypothesized extinct common ancestor that
452 contributed to both *D. cristata* and *D. carthusiana*. *Dryopteris clintoniana* is correctly placed in
453 the major species tree topology, as a grade between *D. cristata* and *D. goldiana*. This
454 reticulation edge from the *Dryopteris* common ancestor may reflect the extinct lineage and a
455 high degree of gene tree variation.

456

457 **DISCUSSION**

458 New phylogenetic network methods offer the promise of elucidating the often complex
459 reticulate histories of polyploid lineages, even in the presence of ILS. Our results demonstrate
460 that phasing polyploid target enrichment data can improve the accuracy of such network
461 inferences as well as divergence time estimates for the networks, and we describe a novel
462 pipeline (PATÉ) to address the difficult problem of phasing polyploid data. Although PATÉ could
463 handle different types of genomic data, such as transcriptomes and whole genomes, target
464 enrichment data are ideal for investigation because they often yield high and even coverage
465 across loci. Because MSC methods assume treat loci independently and assume free
466 recombination between loci, it is not necessary to assign individual loci to parental subgenomes.
467 However, the allele sequences output by PATÉ can also be used as input for the recently
468 developed *Homologizer* (Freyman et al. 2020) or *HybPhaser* (Nauheimer et al. 2020), which
469 attempt to phase across loci and recover parental subgenomes. Our methods also enable
470 population genomic studies of polyploids where accurate estimation of site frequency spectra
471 can be used for demographic analyses otherwise complicated by polyploidy (e.g., Excoffier et
472 al. 2013; Liu and Fu 2020) or SNP-based network inference in the absence of variation suitable
473 for gene tree estimation (Blischak et al 2018; Olave and Meyer 2020).

474

475 **Promises and Pitfalls of Phasing**

476 The prospect of using alleles from phased genomic data presents an exciting step
477 towards revealing the evolutionary history of polyploids, which remains a critical impediment
478 within the plant evolution community (McKain et al. 2018). Strategies for explicitly addressing
479 this challenge are only now emerging (Freyman et al. 2020; Nauheimer et al. 2020), and PATÉ
480 can be a useful tool by phasing variants for many individuals while leveraging genotyping
481 information. Our simulations demonstrate that phasing can improve estimates of reticulate
482 evolutionary relationships using network methods. Phased data can more accurately recover
483 the placement and directionality of hybrid edges than various types of unphased data in
484 simulations (Fig. 4) and empirical analyses with limited numbers of loci (Fig. 7). The advantages
485 of using phased versus unphased data for network estimation decrease when a large number of
486 loci are sampled (Table 1; Fig. 8).

487 Perhaps an underappreciated aspect of phased data is their ability to improve
488 divergence times estimates (Fig. 5; Supplementary Figs. S3-S11; Anderman et al. 2019). Our
489 empirical analyses also demonstrated how the timing of introgression τ_h can be greatly affected
490 by whether phased or consensus data are used. In our *Dryopteris* analyses, the estimate from
491 phased data was nearly four times older than the estimate from unphased data (Supplementary
492 Table S4). The direction of this difference was unanticipated, because our simulations
493 suggested the consensus data should overestimate age compared to phased data. This
494 highlights the difficulties of simulating data that capture real complexities and makes deciding
495 which estimate is more reliable somewhat difficult; however, the uncertainty of τ_h for haplotype
496 consensus data reflected in its posteriors (Supplementary Fig. S14) gives us more confidence in
497 the phased estimates (Supplementary Fig. S12). Because we used the MSci model for
498 divergence time estimation, we did not observe any effect of ILS on age estimates in our
499 simulations, but if we were using concatenation methods to date the divergence times for the

500 allopolyploids two subgenomes, nodes affected by ILS should be overestimated (Tiley et al.
501 2020).

502 In most cases phasing appears to be beneficial, but it may be problematic when the
503 parental lineages are deeply diverged. Although the phased data were able to accurately
504 estimate the age of older speciation nodes (Supplementary Figs. S3-S11), as phylogenetic
505 information is lost from multiple hits, the influence of the prior becomes more substantial. These
506 deep divergence simulation scenarios may border on being biologically unrealistic, as identifying
507 an allopolyploid and its two parental lineages becomes more difficult over time due to extinction
508 and population genetic processes, but it provides some expectations for the performance of
509 phased and unphased data in the presence of high nucleotide divergence. Our simulations
510 showed that when alleles are phased but only one is sampled, as in our pick one simulations,
511 network and divergence time estimation is similar to having all phased alleles present. We also
512 showed where consensus data can perform poorly through simulation (Figs. 3 and 4) as well as
513 empirical analyses where the direction of introgression was more frequently reversed in a
514 simple example of two parental lineages and an allopolyploid (Fig. 8). When enough reads are
515 available to call high-confidence variants, we suggest that phasing with PATÉ can improve
516 network and divergence time estimation for species complexes with low to moderate sequence
517 divergence. However, when investigating very ancient hybrid events, unphased genotype data
518 may be preferential, and using analytical approaches that integrate over phases (Gronau et al.
519 2011; Flouri et al. 2020) may outperform analyses with phased sequences because allele-
520 specific information no longer captures shared ancestry with parental lineages and haplotype
521 blocks become smaller due to recombination.

522

523 ***Challenges of Network Estimation***

524 Our analyses highlight the difficulty of estimating the evolutionary histories of reticulate
525 complexes using phylogenetic methods, regardless of data type. The full-likelihood

526 implementation of the MSci model appears to be useful for limited cases, but these methods are
527 computationally demanding. Thus, they may not be practical for generating hypotheses and
528 exploring unknown relationships for large numbers of taxa (e.g., Zhang et al. 2018). Quartet-
529 based methods are fast and accurate when there are limited numbers of reticulations (Solis-
530 Lemus and Ané 2016) and show similar accuracy to full-likelihood methods for estimating
531 introgression probabilities (Flouri et al. 2020). However, there are scenarios where true network
532 topologies become non-identifiable (Solis-Lemus and Ané 2016). For example, when multiple
533 introgression events affect the same lineage, the expected quartet distribution under the MSci
534 model becomes a poor fit for the empirical data (Cai and Ané 2020) and the network estimated
535 may be incorrect. These effects were evident in our empirical analyses where the relationship
536 between *D. campyloptera*, *D. expansa*, and *D. intermedia* was missing in the nine-species
537 analysis (Fig. 9), which we expect is due to a reticulation edge present between *D. intermedia*
538 and *D. carthusiana*. Phasing sequence data adds information that can improve estimates
539 (Supplementary Table S3), but unsampled or extinct lineages, such as the hypothesized *D.*
540 *semicristata*, can create significant barriers to recovering the true evolutionary history of
541 reticulate complexes, regardless of how many loci or individuals are available.

542

543 ***Insights into Dryopteris Evolution***

544 The North American *Dryopteris* complex has been well-characterized through the study
545 of multi-locus nuclear and chloroplast phylogenies, morphology, cytological observations,
546 chromatography, and isozyme analyses (reviewed in Sessa et al. 2012b). This makes it a useful
547 system for testing our phasing pipeline, and our analyses add nuance to our understanding of
548 some of the relationships among *Dryopteris* species. For example, our results indicate *D.*
549 *campyloptera* has received slightly more loci from *D. intermedia* than *D. expansa* (Fig. 8), and
550 *D. intermedia* is thought to be the likely maternal progenitor (Sessa et al. 2012b). Although our
551 analysis of marginal likelihoods for all target enrichment loci suggested the presence of

552 unsampled ancestral populations (Table 1), the age of introgression and divergence of the *D.*
553 *campyloptera* ancestral population from the *D. intermedia* and *D. expansa* parental lineages is
554 consistent with hybrid speciation rather than a lineage that was isolated from *D. intermedia* and
555 received more recent gene flow from *D. expansa* (Fig. 6). Following the allopolyploidy event, the
556 *D. intermedia* genome was likely dominant, providing some selective advantage for *D.*
557 *campyloptera* in its distribution at the time (Bird et al. 2018). Similar insights can be gained from
558 the nine-taxon analyses, which suggests *D. ludoviciana* is the dominant genome in *D. celsa*.
559 *Dryopteris ludoviciana* is the maternal parent of *D. celsa*, again suggesting some bias in
560 retaining homeologous alleles from the maternal lineage, which provides the chloroplast
561 genome in ferns (Sessa et al. 2012b).

562 The nine-taxon analyses also support the hypothesis of the unsampled diploid lineage *D.*
563 *semicristata*, based on the placement of *D. carthusiana* as sister to the rest of *Dryopteris* in the
564 phased nine-taxon analyses, but with *D. carthusiana* having received over 40% of its genes
565 from *D. intermedia* more recently. Our analyses suggest that *D. cristata* did not have *D.*
566 *ludoviciana* as a progenitor, but rather an unsampled common ancestor of *D. goldiana* and *D.*
567 *ludoviciana*. In the case of *D. cristata*, both parental diploid lineages, including *D. semicristata*,
568 may have gone extinct.

569

570 **Conclusions**

571 Combining phased data with recent network methods holds much promise for
572 confronting a major challenge of plant phylogenetics: resolving the complex histories of
573 polyploids. The PATÉ pipeline can enhance systematic, speciation genomic, and population
574 genomic analyses of groups containing polyploids. While haplotype consensus sequences may
575 be adequate for resolving single reticulation events where both parents are sampled, using
576 phased sequences can improve inferences of more complicated allopolyploid events,
577 demonstrating how allelic variation can be leveraged for MSC methods that account for

578 reticulation. Still, some reticulate complexes can be difficult to disentangle with any data when
579 there are multiple hybrid events involving the same branch. PATÉ is available through GitHub
580 (<https://github.com/gtiley/Phasing>) and can be run on any UNIX environment after installing
581 basic genotyping software and H-PoPG.

582

583 **DATA AVAILABILITY**

584 PATÉ is freely available through GitHub at <https://github.com/gtiley/Phasing>. Simulated
585 and empirical data supporting findings and files for replicating analyses are available from the
586 Dryad Digital Repository: (X). Raw Fastq reads for *Dryopteris* individuals are available through
587 the NCBI SRA database and are associated with BioProject PRJNA725004. Individual SRA
588 Identifiers are available in Supplementary Table S1.

589

590 **SUPPLEMENTARY MATERIAL**

591 Data available from the Dryad Digital Repository: (X).

592

593 **ACKNOWLEDGEMENTS**

594 The authors thank A.M. Duffy, K. Imwattana, M. Nieto-Lugilde, B.T. Piatkowski, and A.J.
595 Shaw for helpful discussions and providing feedback on the manuscript. We also thank M.G
596 Johnson, J. Mendez Reneau, and L. Nauheimer for discussions and sharing their strategies for
597 phasing sequence data. We are grateful to the people who made data collection possible; we
598 used *Dryopteris* samples collected by C.J. Rothfels, M.A. Sundue, and W. Testo, and DNA
599 extractions were performed by S.B. Carey and E. Lockwood.

600

601 **FUNDING**

602 Funding was provided by National Science Foundation awards DEB-2038213 to AAC
603 and PSM, and from DEB-1541506 to JGB and EBS. This work was also partially supported by

604 the Department of Energy award DE-SC0021016 to CSL. ADY and GPT gratefully acknowledge
605 support from Duke University.

606

607

608 **LITERATURE CITED**

- 609 Andermann T., Cano A., Zizka A., Bacon C., Antonelli A. 2018. SECAPR-a bioinformatics
610 pipeline for the rapid and user-friendly processing of targeted enriched Illumina sequences, from
611 raw reads to alignments. *PeerJ* 6:e5175.
612
- 613 Andermann T., Fernandes A.M., Olsson U., Topel M., Pfeil B., Oxelman B., Aleixo A., Faircloth
614 B.C., Antonelli A. 2019. Allele Phasing Greatly Improves the Phylogenetic Utility of
615 Ultraconserved Elements. *Syst. Biol.* 68:32-46.
616
- 617 Baaijens J.A., Schonhuth A. 2019. Overlap graph-based generation of haplotigs for diploids and
618 polyploids. *Bioinformatics* 35:4281-4289.
619
- 620 Bankevich A., Nurk S., Antipov D., Gurevich A.A., Dvorkin M., Kulikov A.S., Lesin V.M.,
621 Nikolenko S.I., Pham S., Pribelski A.D., Pyshkin A.V., Sirotkin A.V., Vyahhi N., Tesler G.,
622 Alekseyev M.A., Pevzner P.A. 2012. SPAdes: a new genome assembly algorithm and its
623 applications to single-cell sequencing. *J. Comput. Biol.* 19:455-477.
624
- 625 Barker M.S., Arrigo N., Baniaga A.E., Li Z., Levin D.A. 2016. On the relative abundance of
626 autopolyploids and allopolyploids. *New Phytol.* 210:391-398.
627
- 628 Beerli P., Mashayekhi S., Sadeghi M., Khodaei M., Shaw K. 2019. Population Genetic Inference
629 With MIGRATE. *Curr. Protoc. Bioinformatics* 68:e87.
630
- 631 Berger E., Yorukoglu D., Peng J., Berger B. 2014. HapTree: a novel Bayesian framework for
632 single individual polyplotyping using NGS data. *PLoS Comput. Biol.* 10:e1003502.
633
- 634 Bezanson J., Edelman A., Karpinski S., Shah V.B. 2015. Julia: A Fresh Approach to Numerical
635 Computing. *arXiv1411.1607v4*.
636
- 637 Bird K.A., VanBuren R., Puzey J.R., Edger P.P. 2018. The causes and consequences of
638 subgenome dominance in hybrids and recent polyploids. *New Phytol.* 220:87-93.
639
- 640 Blischak P.D., Chifman J., Wolfe A.D., Kubatko, L.S. 2018. HyDe: a Python package for
641 genome-scale hybridization detection. *Syst. Biol.*, 67:821-829.
642
- 643 Breinholt J.W., Carey S.B., Tiley G.P., Davis E.C., Endara L., McDaniel S.F., Neves L.G., Sessa
644 E.B., von Konrat M., Chantanaorrapint S., Fawcett S., Ickert-Bond S.M., Labiak P.H., Larraín J.,
645 Lehnert M., Lewis L.R., Nagalingum N.S., Patel N., Rensing S.A., Testo W., Vasco A., Villarreal
646 J.C., Williams E.W., Burleigh J.G. 2021. A target enrichment probe set for resolving the
647 flagellate plant tree of life. *Appl. Plant Sci.* 9:e11406.
648
- 649 Breinholt J.W., Earl C., Lemmon A.R., Lemmon E.M., Xiao L., Kawahara A.Y. 2018. Resolving
650 relationships among the megadiverse butterflies and moths with a novel pipeline for anchored
651 phylogenomics. *Syst. Biol.* 67:78-93.
652
- 653 Buggs J.A., Wendel J.F., Doyle J.J., Soltis D.E., Soltis P.S., Coate J.E. 2014. The legacy of
654 diploid progenitors in allopolyploid gene expression patterns. *Philos. Trans. R. Soc. Lond. B*
655 *Biol. Sci.* 368:20130354.
656

- 657 Cai R., Ané C. 2020. Assessing the fit of the multi-species network coalescent to multi-locus
658 data. *Bioinformatics* btaa863. doi: <https://doi.org/10.1093/bioinformatics/btaa863>
659
- 660 Colle M., Leisner C.P., Wai C.M., Ou S., Bird K.A., Wang J., Wisecaver J.H., Yocca A.E., Alger
661 E.I., Tang H., Xiong Z., Callow P., Ben-Zvi G., Brodt A., Baruch K., Swale T., Shiue L., Song G.-
662 Q., Childs K.L., Schillmiller A., Vorsa N., Buell C.R., VanBuren R., Jiang N., Edger P.P. 2019.
663 Haplotype-phased genome and evolution of phytonutrient pathways of tetraploid blueberry.
664 *GigaScience* 8:giz012.
665
- 666 Crowl A.A., Myers C., Cellinese N. 2017. Embracing discordance: Phylogenomic analyses
667 provide evidence for allopolyploidy leading to cryptic diversity in a Mediterranean Campanula
668 (Campanulaceae) clade. *Evolution* 71:913-922.
669
- 670 DePristo M., Banks E., Poplin R., Garimella K., Maguire J., Hartl C., Philippakis A., del Angel G.,
671 Rivas M.A., Hanna M., McKenna A., Fennell T., Kernysky A., Sivachenko A., Cibulskis K.,
672 Gabriel S., Altschuler S., Daly M. 2011. A framework for variation discovery and genotyping
673 using next-generation DNA sequencing data. *Nat. Genet.* 43:491-498.
674
- 675 Edgar R.C. 2004. MUSCLE: multiple sequence alignment with high accuracy and high
676 throughput. *Nucleic Acids Res.* 32:1792-1797.
677
- 678 Eriksson J.S., de Sousa F., Bertrand Y.J.K., Antonelli A., Oxelman B., Pfeil B.E. 2018. Allele
679 phasing is critical to revealing a shared allopolyploid origin of *Medicago arborea* and *M.*
680 *strasseri* (Fabaceae). *BMC Evol. Biol.* 18:9.
681
- 682 Excoffier L., Dupanloup I., Huerta-Sanchez E., Sousa V.C., Foll M. 2013. Robust demographic
683 inference from genomic and SNP data. *PLoS Genet.* 9:e1003905.
684
- 685 Faircloth B.C. 2016. PHYLUCE is a software package for the analysis of conserved genomic
686 loci. *Bioinformatics* 32:786-788.
687
- 688 Faircloth B.C., McCormack J.E., Crawford N.G., Harvey M.G., Brumfield R.T., Glenn T.C. 2012.
689 Ultraconserved elements anchor thousands of genetic markers spanning multiple evolutionary
690 timescales. *Syst. Biol.* 61:717-726.
691
- 692 Farhat P., Hidalgo O., Robert T., Siljak-Yakovlev S., Leitch I.J., Adams R.P., Bou Dagher-
693 Kharrat M. 2019. Polyploidy in the Conifer Genus *Juniperus*: An Unexpectedly High Rate. *Front.*
694 *Plant Sci.* 10:676.
695
- 696 Flouri T., Jiao X., Rannala B., Yang Z. 2020. A Bayesian Implementation of the Multispecies
697 Coalescent Model with Introgression for Phylogenomic Analysis. *Mol. Biol. Evol.* 37:1211-1223.
698
- 699 Flouri T., Jiao X., Rannala B., Yang Z.. 2018. Species Tree Inference with BPP Using Genomic
700 Sequences and the Multispecies Coalescent. *Mol. Biol. Evol.* 35:2585-2593.
701
- 702 Freyman W.A., Johnson M.G., Rothfels C.J. 2020. Homologizer: Phylogenetic phasing of gene
703 copies into polyploid subgenomes. *bioRxiv* doi: <https://doi.org/10.1101/2020.10.22.351486>.
704
- 705 Gronau I., Hubisz M.J., Gulko B., Danko C.G., Siepel A. 2011. Bayesian inference of ancient
706 human demography from individual genome sequences. *Nat. Genet.* 43:1031-1034.
707

- 708 He D., Saha S., Finkers R., Parida L. 2018. Efficient algorithms for polyploid haplotype phasing.
709 *BMC Genomics* 19:110.
710
- 711 Huang J., Flouri T., Yang Z. 2020. A simulation study to examine the information content in
712 phylogenomic datasets under the multispecies coalescent model. *Mol. Biol. Evol.* 37:3211-3224.
713
- 714 Huber K.T., Oxelman B., Lott M., Moulton V. 2006. Reconstructing the evolutionary history of
715 polyploids from multi-labelled trees. *Mol. Biol. Evol.* 23:1784-1791.
716
- 717 Hudson R.R. 1983. Testing the Constant-Rate Neutral Allele Model with Protein Sequence
718 Data. *Evolution* 37:203-217.
719
- 720 Huson D.H., Rupp R., Scornavacca C. 2010. Phylogenetic networks: concepts, algorithms and
721 applications. Cambridge University Press.
722
- 723 Iqbal Z., Caccamo M., Turner I., Flicek P., McVean G. 2012. De novo assembly and genotyping
724 of variants using colored de Bruijn graphs. *Nat. Genet.* 44:226-232.
725
- 726 Jantzen J.R., Amarasinghe P., Folk R.A., Reginato M., Michelangeli F.A., Soltis D.E., Cellinese
727 N., Soltis P.S. 2020. A two-tier bioinformatic pipeline to develop probes for target capture of
728 nuclear loci with applications in Melastomataceae. *Appl. Plant Sci.* 8:e11345.
729
- 730 Johnson M.G., Gardner E.M., Liu Y., Medina R., Goffinet B., Shaw A.J., Zerega N.J., Wickett
731 N.J. 2016. HybPiper: Extracting coding sequence and introns for phylogenetics from high-
732 throughput sequencing reads using target enrichment. *Appl. Plant Sci.* 4:1600016.
733
- 734 Johnson M.G., Pokorny L., Dodsworth S., Botigue L.R., Cowan R.S., Devault A., Eiserhardt
735 W.L., Epitawalage N., Forest F., Kim J.T., Leebens-Mack J.H., Leitch I.J., Maurin O., Soltis
736 D.E., Soltis P.E., Wong G.K.-S., Baker W.J., Wickett N.J. 2019. A Universal Probe Set for
737 Targeted Sequencing of 353 Nuclear Genes from Any Flowering Plant Designed Using k-
738 Medoids Clustering. *Syst. Biol.* 68:594-606.
739
- 740 Jones G., Sagitov S., Oxelman B. 2013. Statistical inference of allopolyploid species networks in
741 the presence of incomplete lineage sorting. *Syst. Biol.* 62:467-478.
742
- 743 Jukes T.H., Cantor C.R. 1969. Evolution of protein molecules. In: Munro H.N., editor.
744 Mammalian Protein Metabolism. New York, NY: Academic Press. p. 21-132.
745
- 746 Kalyaanamoorthy S., Minh B.Q., Wong T.K.F., von Haeseler A., Jermini L.S. 2017.
747 ModelFinder: fast model selection for accurate phylogenetic estimates. *Nat. Methods* 14:587-
748 589.
749
- 750 Karimi N., Grover C.E., Gallagher J.P., Wendel J.F., Ané C., Baum D.A. 2020. Reticulate
751 Evolution Helps Explain Apparent Homoplasy in Floral Biology and Pollination in Baobabs
752 (*Adansonia*; Bombacoideae; Malvaceae). *Syst. Biol.* 69:462-478.
753
- 754 Kates H.R., Johnson M.G., Gardner E.M., Zerega N.J.C., Wickett N.J. 2018. Allele phasing has
755 minimal impact on phylogenetic reconstruction from targeted nuclear gene sequences in a case
756 study of *Artocarpus*. *Am. J. Bot.* 105:404-416.
757

- 758 Lemmon A.R., Emme S.A., Lemmon E.M. 2012. Anchored hybrid enrichment for massively
759 high-throughput phylogenomics. *Syst. Biol.* 61:727-744.
760
- 761 Li H., Durbin R. 2009. Fast and accurate short read alignment with Burrows-Wheeler transform.
762 *Bioinformatics* 25:1754-1760.
763
- 764 Liu X., Fu Y.X. 2020. Stairway Plot 2: demographic history inference with folded SNP frequency
765 spectra. *Genome Biol.* 21:280.
766
- 767 Liu Y., Johnson M.G., Cox C.J., Medina R., Devos N., Vanderpoorten A., Hedenas L., Bell N.E.,
768 Shevock J.R., Aguero B., Quandt D., Wickett N.J., Shaw A.J., Goffinet B. 2019. Resolution of
769 the ordinal phylogeny of mosses using targeted exons from organellar and nuclear genomes.
770 *Nat. Commun.* 10:1485.
771
- 772 Lott M., Spillner A., Huber K.T., Moulton V. 2009. PADRE: a package for analyzing and
773 displaying reticulate evolution. *Bioinformatics* 25:1199-1200.
774
- 775 Luo R., Liu B., Xie Y., Li Z., Huang W., Yuan J., He G., Chen Y., Pan Q., Liu Y., Tang J., Wu G.,
776 Zhang H., Shi Y., Liu Y., Yu C., Wang B., Lu Y., Han C., Cheung D.W., Yiu S.-M., Peng S.,
777 Xiaoqian Z., Liu G., Liao X., Li Y., Yang H., Wang J., Lam T-W., Wang J. 2012. SOAPdenovo2:
778 an empirically improved memory-efficient short-read de novo assembler. *GigaScience* 1:18.
779
- 780 McKain M.R., Johnson M.G., Uribe-Convers S., Eaton D., Yang Y. 2018. Practical
781 considerations for plant phylogenomics. *Appl. Plant Sci.* 6:e1038.
782
- 783 McKenna A., Hanna M., Banks E., Sivachenko A., Cibulskis K., Kernytsky A., Garimella K.,
784 Altshuler D., Gabriel S., Daly M., DePristo M.A. 2010. The Genome Analysis Toolkit: a
785 MapReduce framework for analyzing next-generation DNA sequencing data. *Genome Res.*
786 20:1297-1303.
787
- 788 Moeinzadeh M.H., Yang J., Muzychenko E., Gallone G., Heller D., Reinert K., Haas S., Vingron
789 M. 2020. Ranbow: A fast and accurate method for polyploid haplotype reconstruction. *PLoS*
790 *Comput. Biol.* 16:e1007843.
791
- 792 Montgomery J.D., Paulton E.M. 1981. *Dryopteris* in North America. *Fiddlehead Forum* 8:25-31.
793
- 794 Morales-Briones D.F., Liston A., Tank D.C. 2018. Phylogenomic analyses reveal a deep history
795 of hybridization and polyploidy in the Neotropical genus *Lachemilla* (Rosaceae). *New Phytol.*
796 218:1668-1684.
797
- 798 Nauheimer L., Weigner N., Joyce E., Crayn D., Clarke C., Nargar K. 2020. HybPhaser: a
799 workflow for the detection and phasing of hybrids in target capture datasets. bioRxiv. doi:
800 <https://doi.org/10.1101/2020.10.27.354589>.
801
- 802 Nguyen L.-T., Schmidt H.A., von Haeseler A., Minh B.Q. 2015. IQ-TREE: a fast and effective
803 stochastic algorithm for estimating maximum-likelihood phylogenies. *Mol. Biol. Evol.* 32:268-
804 274.
805
- 806 Oberprieler C., Wagner F., Tomasello S., Konowalik K. 2017. A permutation approach for
807 inferring species networks from gene trees in polyploid complexes by minimising deep
808 coalescences. *Methods in Ecology and Evolution* 8:835-849.

- 809
810 Olave M., Meyer A. 2020. Implementing Large Genomic Single Nucleotide Polymorphism Data
811 Sets in Phylogenetic Network Reconstructions: A Case Study of Particularly Rapid Radiations of
812 Cichlid Fish. *Syst. Biol.* 69:848-862.
813
814 Pamilo P., Nei M. 1988. Relationships between gene trees and species trees. *Mol. Biol. Evol.*
815 5:568-583.
816
817 Rothfels C.J., Pryer K.M., Li F.-W. 2017. Next-generation polyploid phylogenetics: rapid
818 resolution of hybrid polyploid complexes using PacBio single-molecule sequencing. *New Phytol.*
819 213:413-429.
820
821 Saada O.A., Tsouris A., Freidrich A., Schachrer J. 2020. nPhase: An accurate and contiguous
822 phasing method for polyploids. *bioRxiv* doi:<https://doi.org/10.1101/2020.07.24.219105>.
823
824 Sessa E.B., Zimmer E.A., Givnish T.J. 2012a. Reticulate evolution on a global scale: a nuclear
825 phylogeny for New World Dryopteris (Dryopteridaceae). *Mol. Phylogenet. Evol.* 64:563-581.
826
827 Sessa E.B., Zimmer E.A., Givnish T.J. 2012b. Unraveling reticulate evolution in North American
828 Dryopteris (Dryopteridaceae). *BMC. Evol. Biol.* 12:104.
829
830 Solis-Lemus C., Ané C. 2016. Inferring Phylogenetic Networks with Maximum Pseudolikelihood
831 under Incomplete Lineage Sorting. *PLoS Genet.* 12:e1005896.
832
833 Solis-Lemus C., Bastide P., Ané C. 2017. PhyloNetworks: A Package for Phylogenetic
834 Networks. *Mol. Biol. Evol.* 34:3292-3298.
835
836 Soltis, D.E., Visger C.J., Soltis P.S. 2014. The polyploidy revolution then...and now: Stebbins
837 revisited. *American Journal of Botany* 101: 1057–1078.
838
839 Stull G.W., Soltis P.S., Soltis D.E., Gitzendanner M.A., Smith S.A. 2020. Nuclear phylogenomic
840 analyses of asterids conflict with plastome trees and support novel relationships among major
841 lineages. *Am. J. Bot.* 107:790-805.
842
843 Tiley G.P., Poelstra J.W., dos Reis M., Yang Z., Yoder A.D. 2020. Molecular Clocks without
844 Rocks: New Solutions for Old Problems. *Trends Genet.* 36:845-856.
845
846 Viruel J., Conejero M., Hidalgo O., Pokorny L., Powell R.F., Forest F., Kantar M.B., Soto Gomez
847 M., Graham S.W., Gravendeel B., Wilkin P., Leitch I.J. 2019. A Target Capture-Based Method
848 to Estimate Ploidy from Herbarium Specimens. *Front. Plant Sci.* 10:937.
849
850 Weiss C.L., Pais M., Cano L.M., Kamoun S., Burbano H.A. 2018. nQuire: a statistical framework
851 for ploidy estimation using next generation sequencing. *BMC Bioinformatics* 19:122.
852
853 Wen D., Yu Y., Nakhleh L. 2016. Bayesian Inference of Reticulate Phylogenies under the
854 Multispecies Network Coalescent. *PLoS Genet.* 12:e1006006.
855
856 Wen D., Yu Y., Zhu J., Nakhleh L. 2018. Inferring Phylogenetic Networks Using PhyloNet. *Syst.*
857 *Biol.* 67:735-740.
858

- 859 Wolf P.G., Robison T.A., Johnson M.G., Sundue M.A., Testo W.L., Rothfels C.J. 2018. Target
860 sequence capture of nuclear-encoded genes for phylogenetic analysis in ferns. *Appl. Plant Sci.*
861 6:e01148.
862
- 863 Wood T.E., Takebayashi N., Barker M.S., Mayrose I., Greenspoon P.B., Rieseberg L.H. 2009.
864 The frequency of polyploid speciation in vascular plants. *Proc. Natl. Acad. Sci. U. S. A.*
865 106:13875-13879.
866
- 867 Xie M., Wu Q., Wang J., Jiang T. 2016. H-PoP and H-PoPG: heuristic partitioning algorithms for
868 single individual haplotyping of polyploids. *Bioinformatics* 32:3735-3744.
869
- 870 Xie W., Lewis P.O., Fan Y., Kuo L., Chen M.H. 2011. Improving marginal likelihood estimation
871 for Bayesian phylogenetic model selection. *Syst. Biol.* 60:150-160.
872
- 873 Yang J., Moeinzadeh M-H., Kuhl H., Helmuth J., Xiao P., Haas S., Liu G., Zheng J., Sun Z., Fan
874 W., Deng G., Wang H., Hu F., Zhao S., Fernie A.R., Boerno S., Timmermann B., Zhang P.,
875 Vingron M. 2017. Haplotype-resolved sweet potato genome traces back its hexaploidization
876 history. *Nat Plants* 3:696-703.
877
- 878 Yang Z. 2006. Computational molecular evolution: Oxford University Press.
879
- 880 Zhang C., Ogilvie H.A., Drummond A.J., Stadler T. 2018. Bayesian Inference of Species
881 Networks from Multilocus Sequence Data. *Mol. Biol. Evol.* 35:504-517.
882
- 883 Zhang C., Rabiee M., Sayyari E., Mirarab S. 2018. ASTRAL-III: polynomial time species tree
884 reconstruction from partially resolved gene trees. *BMC Bioinformatics* 19:153.
885
- 886 Zhu S., Degnan J.H. 2017. Displayed trees do not determine distinguishability under the
887 network multispecies coalescent. *Syst. Biol.* 66:283-298.
888

889 TABLES

Topology	Phased Marginal lnL	Unphased Marginal lnL	Phased Model Probability	Unphased Model Probability
1	-613405.3154	-552720.6776	1.006E-278	3.2574E-214
2	-613223.0755	-552534.6540	1.4073E-199	2.0039E-133
3	-613366.4128	-552644.7603	7.9026E-262	3.0431E-181
4	-612866.6368	-552245.2218	8.86633E-45	1.00164E-07
5	-612828.7348	-552243.7091	2.56082E-28	4.54611E-07
6	-612822.4509	-552238.6462	1.37227E-25	7.18535E-05
7 [†]	-612765.2027	-552229.1054	1	0.999927592
8	-613211.8583	-552484.8320	1.047E-194	8.6956E-112
9	-613168.7562	-552479.3732	5.4825E-176	2.0419E-109
10	-613102.1509	-552454.2002	4.6266E-147	1.74796E-98
11	-613079.9316	-552426.8867	2.0654E-137	1.27244E-86
12	-613379.6350	-552538.6937	1.4303E-267	3.5276E-135
13	-613390.9585	-552533.6798	1.7287E-272	5.3085E-133
14	-613272.7561	-552561.3165	3.7359E-221	5.2787E-145
15	-613247.7503	-552566.6741	2.7054E-210	2.4873E-147

890

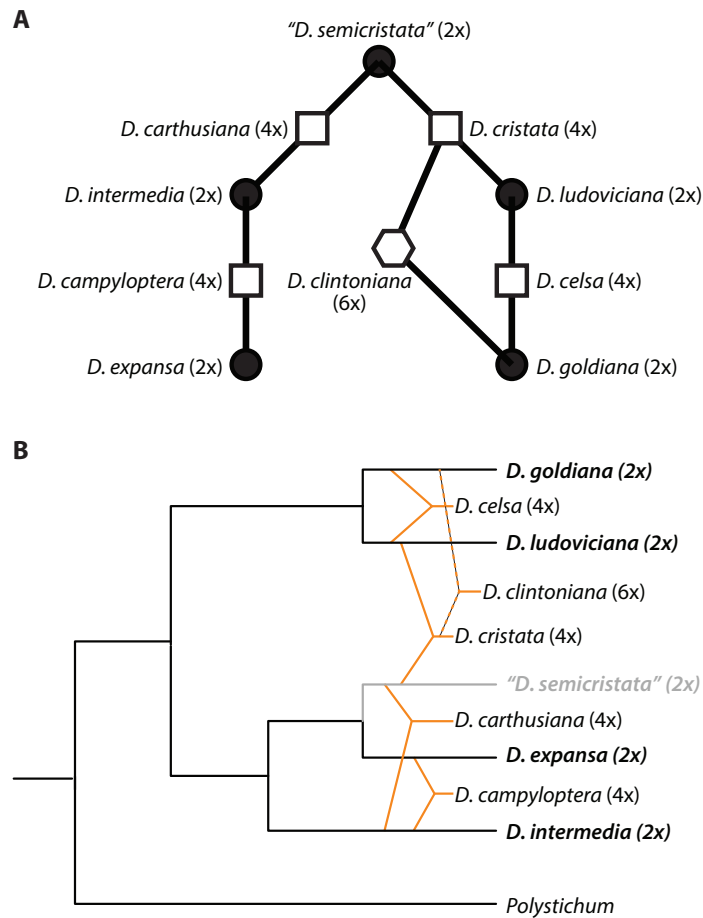
891 **Table 1 — Marginal Likelihoods for Possible Topological Hypotheses.** Topologies of the 15

892 models are displayed in Figure S1.

893 [†]*a priori* allopolyploid hypothesis

894

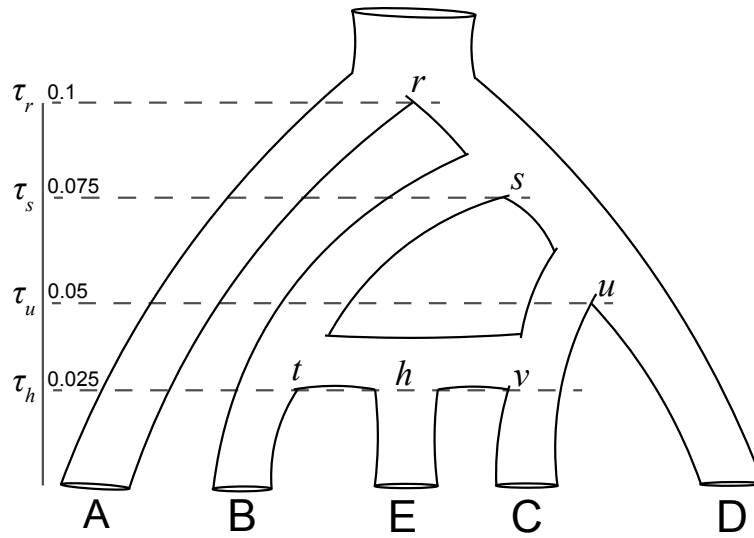
895 **FIGURES**



896

897 **Figure 1 — Hypothesized Relationships among North American *Dryopteris*.** Synthesis of
 898 results from Sessa et al. 2012a and Sessa et al. 2012b. A) Links between shapes show the
 899 putative parents and their allopolyploid derivatives. Black circles are diploids, squares are
 900 tetraploids, and the hexagon is the one hexaploid species in the group. *Dryopteris semicristata*
 901 is presumed extinct. B) Placement of allopolyploids in the context of the backbone relationships
 902 among diploids. Tetraploids are indicated with solid orange lines and the hexaploid with dotted
 903 lines. The grey line denoting a sister relationship between *D. semicristata* and *D. expansa*
 904 reflects one possible placement for the extinct taxon based on previous analyses (Sessa et al.,
 905 2012b).

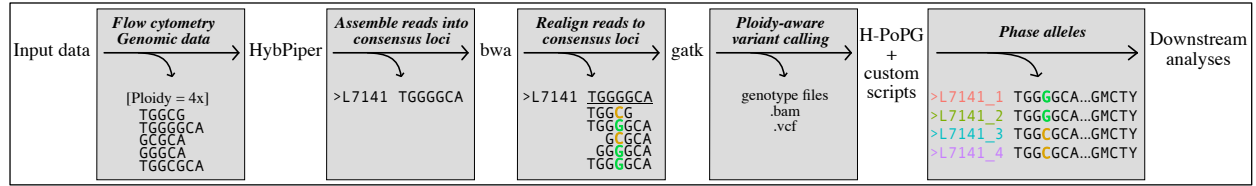
906



907

908 **Figure 2 — Species network used for simulation.** The divergence times in expected
909 substitutions per site are given for each node, and h is the hybrid node where two alleles enter
910 from both t and v . E is an allotetraploid while other species are diploid. Nucleotide divergence
911 was reduced by dividing all τ by 10 or increased by multiplying all τ by 10. ILS was increased by
912 halving the distance between τ_h and τ_u and between τ_u and τ_s either once (for the medium ILS
913 condition) or twice (for the high ILS condition).

914



915

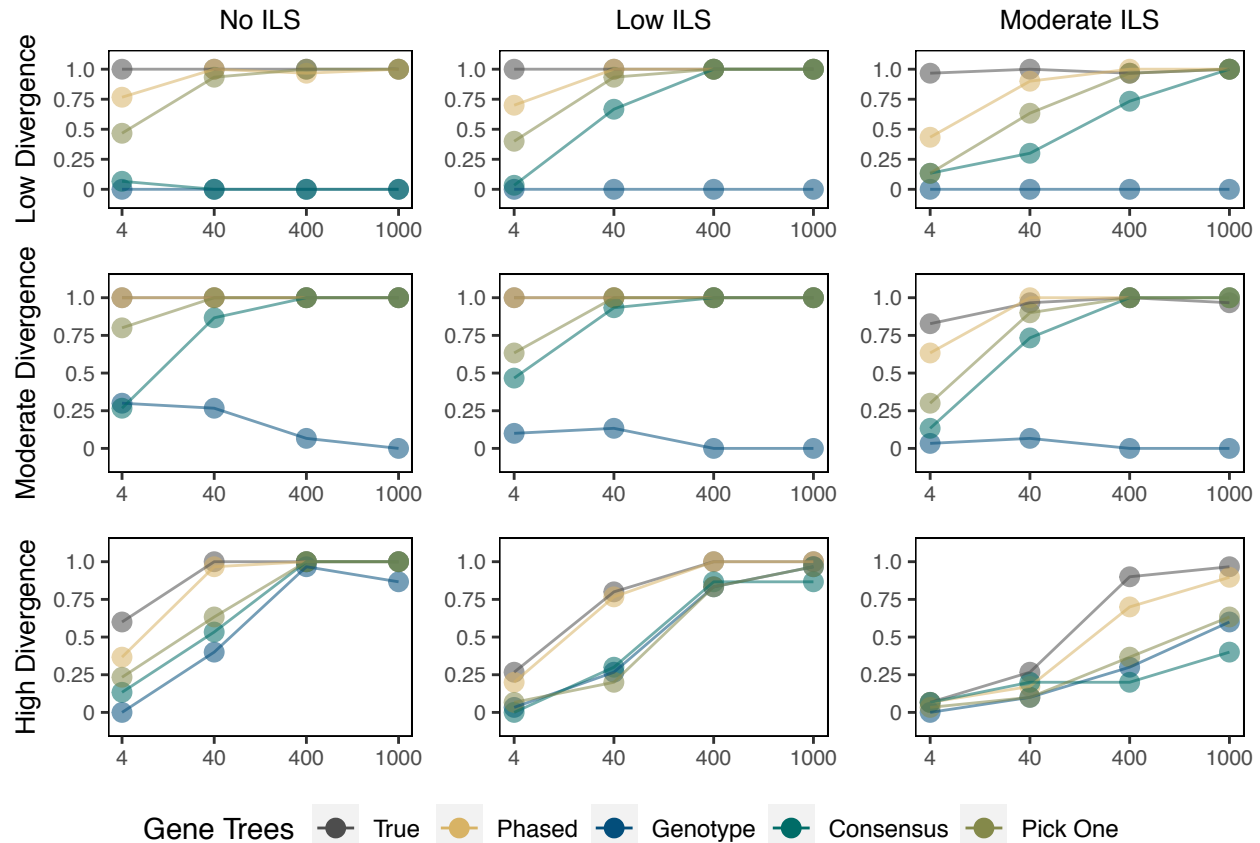
916 **Figure 3 — PATÉ Phasing Pipeline.** Overview of data input, output, and steps taken to phase

917 alleles. Input data are assumed to be paired-end Illumina reads and reference sequences for

918 each individual are required (consensus loci from HybPiper can be used). The ploidy of each

919 individual must be specified. Only biallelic sites are used for phasing.

920



921

922 **Figure 4 — Proportion of simulations that correctly identify the allopolyploid lineage.** The

923 x-axes are the number of loci sampled for each simulation. The y-axes are the proportions of

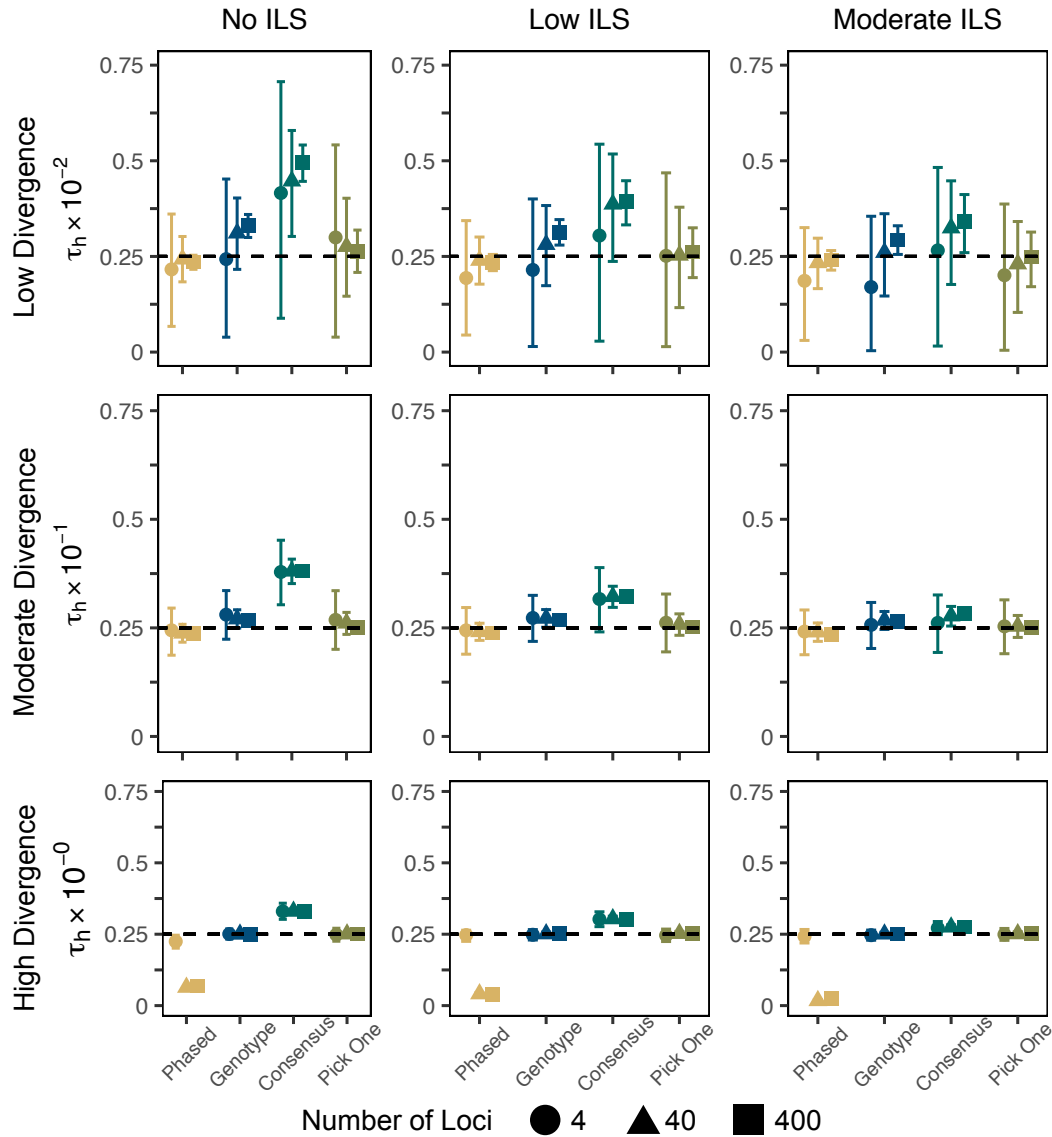
924 correct networks. Results are based on networks estimated with a single reticulation, even if

925 that network was considered less optimal than networks with zero or two reticulations. We

926 saved the true gene trees from the simulations, while we estimated gene trees with the phased

927 and unphased (Genotype, Consensus, and Pick One) data.

928



929

930 **Figure 5 — Estimating the Timing of Introgression.** Divergence times are for node h in

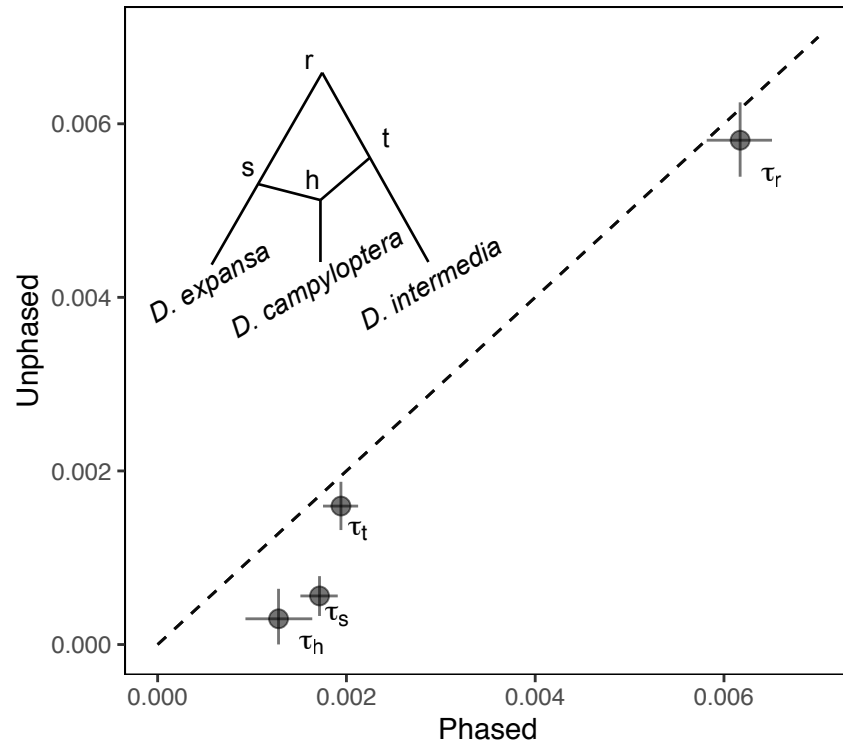
931 Figure 2. The low divergence simulation corresponds to the y-axis units of $\tau_h \times 10^{-2}$ while the

932 high divergence case is represented by τ_h . Divergence times are measured as the expected

933 number of substitutions per site. The dashed line represents the true simulated values. Points

934 are posterior means, and error bars are 95% HPD intervals, averaged across 30 replicates.

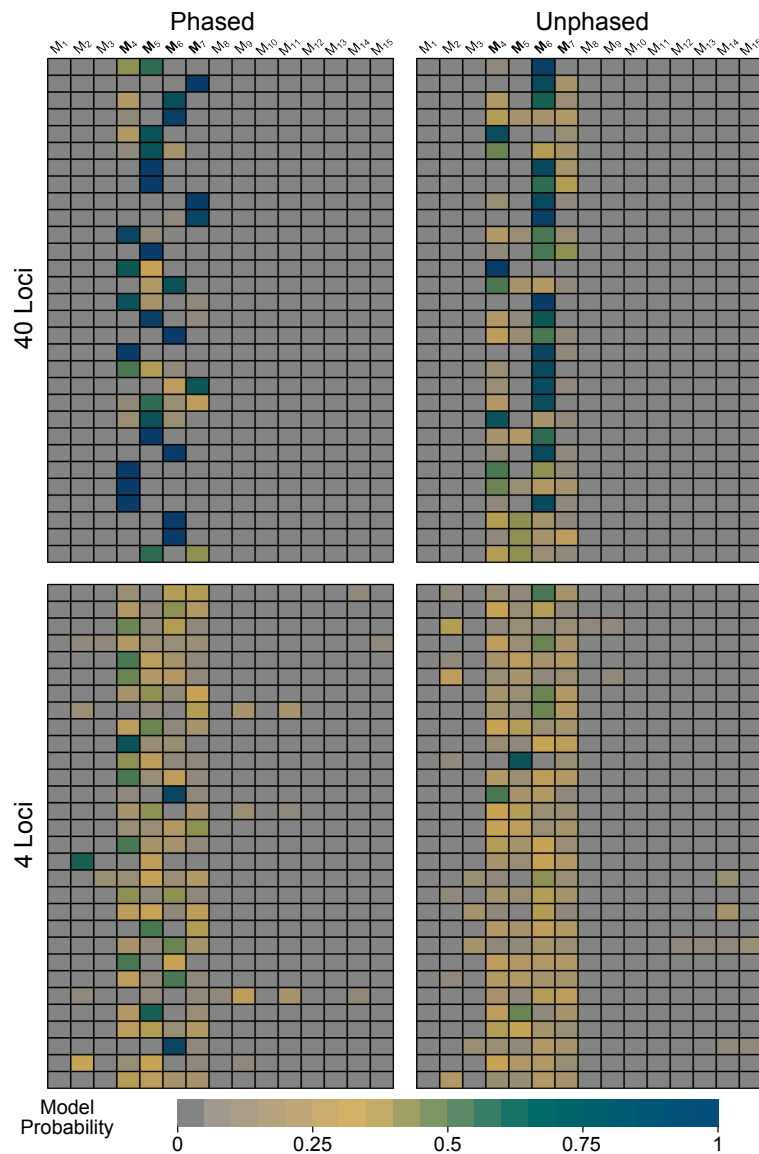
935



936

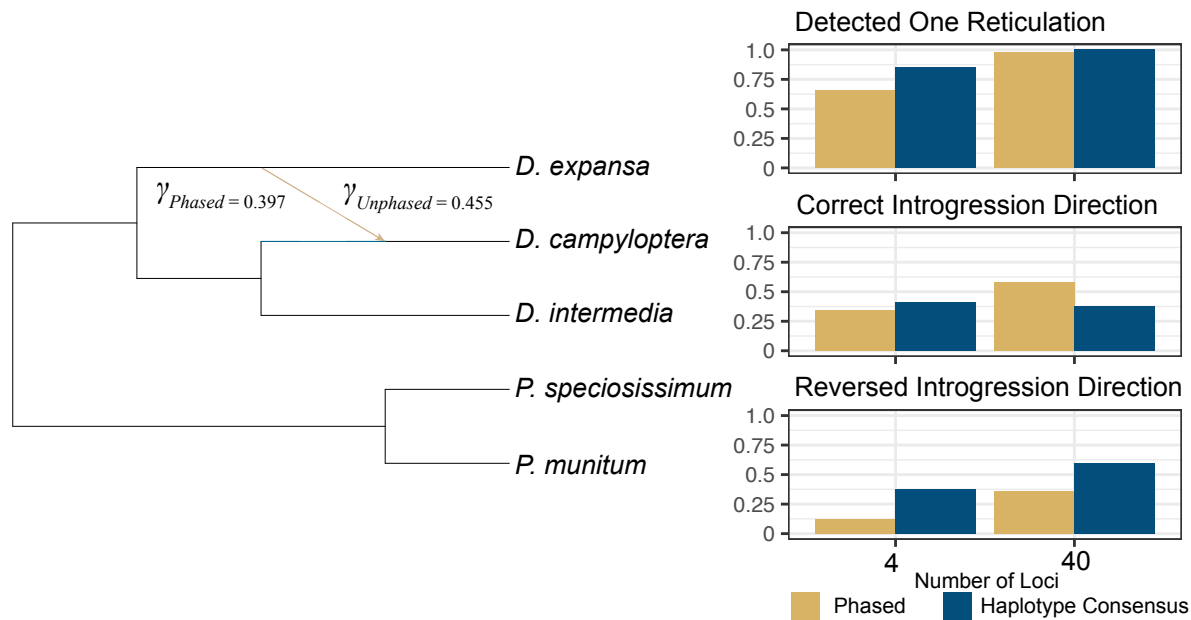
937 **Figure 6— *Dryopteris* Divergence Times under the MSci Model.** Divergence times are
938 measured as the expected number of substitutions per site. The x-axis shows estimates from
939 phased data and the y-axis shows estimates from unphased (haplotype consensus) data for the
940 inset network (equivalent to model 7 from Supplementary Fig. S1). The dashed one-to-one line
941 shows where older age estimates are consistently obtained from phased data. Error bars on
942 points show the 95% HPD intervals for phased and unphased data.

943



944

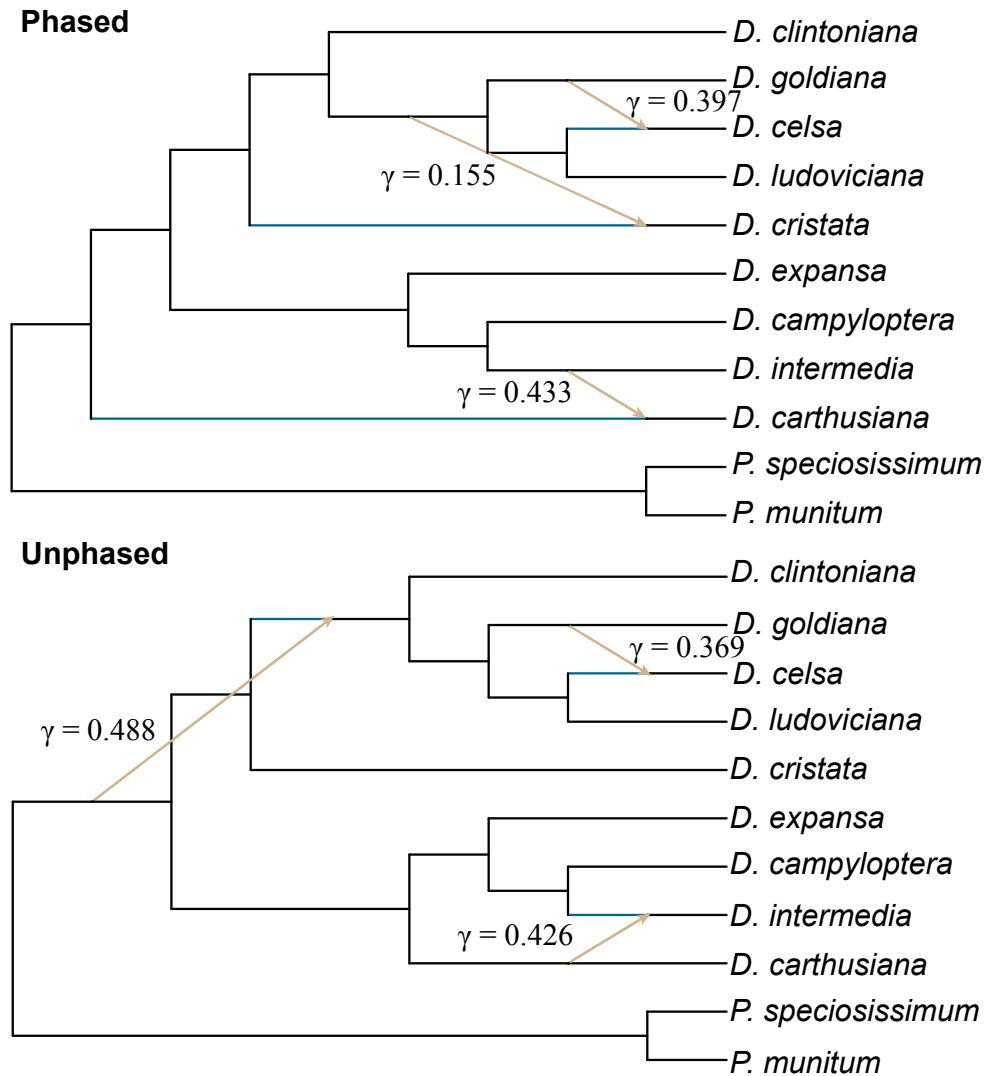
945 **Figure 7— Probabilities for three-taxon *Dryopteris* MSci Models with fewer Loci.** Marginal
 946 likelihoods were estimated for the 15 MSci models (Supplementary Fig. S1). Model weights
 947 were used to obtain probabilities. We consider model probability greater than 0.95 as decisive
 948 evidence in favor of a model, and a probability less than 0.05 is evidence against a model. We
 949 considered probabilities between 0.05 and 0.95 to be ambiguous. Models four through seven (in
 950 bold) all have the correct reticulate relationships between the parental diploid lineages and the
 951 allopolyploid. Models one through three do not have introgression, and models eight through 15
 952 have incorrect introgression events. Each row represents one of 30 sampling replicates.



953

954 **Figure 8 — Network search results for three-taxon *Dryopteris* example.** Both phased and
 955 unphased haplotype consensus data recovered the same network topology with introgression
 956 occurring in the expected direction. The major topology is indicated by the blue edge and the
 957 minor edge (direction of introgression) is shown in tan. The inheritance probability γ was slightly
 958 higher in the haplotype consensus data ($\gamma_{\text{unphased}} = 0.455$). Bar plots show the proportion of
 959 100 replicates when sampling four or 40 loci that correctly detect one reticulation based on the
 960 pseudolikelihood scores (top), correctly estimate the network with introgression going from one
 961 of the diploids into *D. campyloptera* (middle), and estimate a network where the direction of
 962 introgression is from *D. campyloptera* into one of the diploids (bottom).

963



964

965 **Figure 9 — Networks for Nine-Taxon *Dryopteris* example.** Both data types recovered
 966 optimal networks with three reticulation events. The major topology edge is blue and the minor
 967 (reticulation) edges shown in tan, with the direction of introgression flowing into the major edge.
 968 The position of *D. carthusiana* changes in the major topology between phased and unphased
 969 data but the relationships are otherwise the same. All three reticulation events in the phased
 970 data are plausible, but in the unphased data, the direction of introgression from *D. carthusiana*
 971 into *D. intermedia* is incorrect and the reticulate edge from the common ancestor of *Dryopteris* is
 972 difficult to reconcile. Inheritance probabilities for each introgression event are shown next to
 973 reticulation edges.